

Active Nematics at Bifurcations

Zhengyang Liu,¹ Claire Doré,¹ Antonio Tavera-Vazquez,^{1,2} and Teresa Lopez-Leon¹

¹Laboratoire Gulliver, UMR 7083 CNRS, ESPCI Paris, PSL Research University, 75005 Paris, France.

²Pritzker School of Molecular Engineering, University of Chicago, Chicago, IL 60637, USA.

(Dated: December 5, 2024)

Under lateral confinement, active matter self-organize into coherent flows. Such behavior implies the possibility of achieving logical operations in properly designed channel networks. Bifurcations are a key ingredient in channel networks. Understanding active matter behavior at bifurcations is therefore an important step towards a proper channel network design. In this paper, we experimentally explore active matter behavior at bifurcations using the microtubule-kinesin model system. Specifically, we compare the effects of channel length, ratchets and turning angles. Our results suggest that ratchets and turning angles help establish unambiguous polarized flow states. In contrast, channel length is a less relevant factor, which results in more frequently changing flow states. Our experiment is the first step to understanding active nematic flows in complex channel networks. The result lays the foundation for active matter logic and computation.

I. INTRODUCTION

Active matter flows spontaneously under channel confinement, forming coherent flows [1–5]. Such behavior implies several possible applications of active matter, including serving as micro-scale transport, soft robotics and active matter logic [6, 7]. Boundary-mediated control has been shown effective in manipulating active matter in both experiments [1–4, 8–10] and simulations [11–14]. As of now, most studies have focused on the behavior of active matter in stand-alone smooth channels, which showed that active flows were intrinsically bistable [2, 3]. However, to realize the full potential of active matter channel flows, it is necessary to study the behavior of active matter in channel networks and with asymmetric geometries, as suggested by the pioneering theoretical work on active matter logic [7]. Very recently, channel networks attract more attention, and frustrated flow states have been investigated in coupled annular rings [5] and large honeycomb-like networks [15]. The other essential component of active matter logic is the diode channel, which only permits flow in one direction. While a few early works have hinted or employed asymmetric geometries, such as a kink or an array of ratchet teeth, to steer active matter flows [2, 5, 14, 16–18], a systematic study of asymmetric channels in the context of channel networks, especially frustrated flow states, is still missing.

In this work, we filled this gap by experimentally studying the flow behavior of active matter at channel networks consisting of asymmetric channels. To obtain a clear understanding, we studied the simplest possible form of a channel network – the bifurcation – where three channels are connected to one node. Despite of being simple, the bifurcation is a key element of more complex channel networks, and a great system to observe frustrated flow states. Assymetry are in two levels: in single channel level, ratchets are introduced to favor the flow in a certain direction; in network level, input channels are designed to split into channels with different lengths, number of ratchets and turning angles. Our results sug-

gest that ratchets and turning angles help establish stable polarized flow states, where the inlet flow primarily goes into one of the outlet channels, leaving the other channel with little flow. In contrast, channel length is a less relevant factor, which results in more frequently changing flow states. The topological defects show different dynamics in flowing ratchet channels from frustrated straight channels, uncovering the steering mechanism of the ratchets. Our experiment is the first step to understanding active nematic flows in complex channel networks. The result lays the foundation for potential applications of active flow networks in mass transport and flow computation.

II. EXPERIMENT

Our active matter system comprises microtubule filaments powered by ATP-consuming two-headed kinesin molecular motors [19]. By adding depleting agent poly ethylene glycol (PEG), the system forms dense bundles at the water-oil interface. Driven by the kinesin motors, the bundles stretch and bend constantly, exhibiting chaotic flows characterized by the formation and annihilation of topological defects. In an experiment, 2.5 μ L of microtubule solution was put in a custom pool of 5 mm diameter, covered by 100 μ L of silicone oil (5 cSt). The micro-printed bifurcation channel structure was then gently placed at the oil-water interface, confining the chaotic system into channel flows (Fig. 1(a)). An unconfined active nematics system is shown in Fig. 1(b), while the same system confined by the bifurcation channels is shown in Fig. 1(c). The active nematics system is observed using a confocal microscope (Nikon), and images are taken at 2 Hz using a 10X objective lens. Then, 400 μ m of each channel is cropped and analyzed by PIV, as shown in Fig. 2(a).

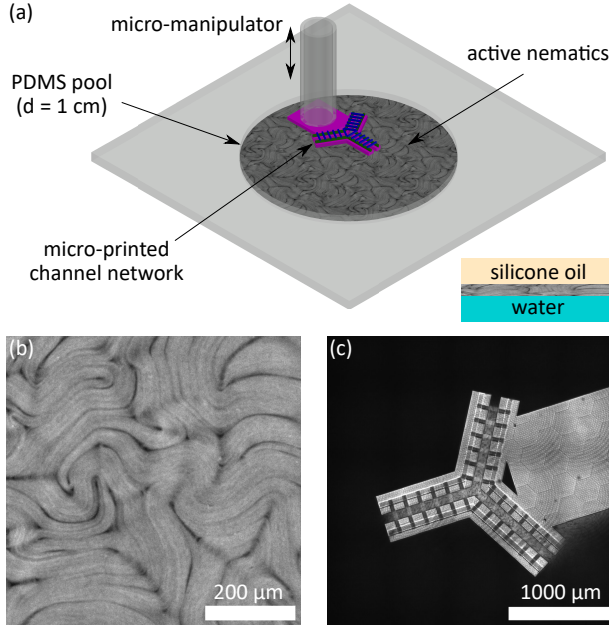


FIG. 1. Confining microtubule-kinesin system at water-oil interface – the experimental setup. (a) Schematic diagram of the experimental setup. The microtubule-kinesin active nematic system is placed at an water-oil interface in a custom PDMS pool, and is subject to lateral confinement by the micro-printed bifurcation channel. (b) Confocal image of a mature interfacial microtubule-kinesin system. (c) Confocal image of the bifurcation channels set on the interfacial microtubule-kinesin system.

III. RESULTS

A. Symmetric bifurcation

We first studied the flow behavior at a symmetric bifurcation, where all the channels are smooth and of the same length. To extract the flow rate in each channel, we cropped regions 400 μm from the connecting node for each channel and performed Particle Image Velocimetry (PIV) analysis (as indicated by the rectangles in Fig. 2(a)). Snapshots of the PIV results are shown in Fig. 2(b). Local velocity vectors $v(x, y)$ are indicated as yellow arrows, where x and y are defined separately as the transverse and parallel directions for each channel, respectively.

The surface flow rate in the channel direction (Q_y) was calculated by integrating the velocity field over the channel cross-section. To minimize the noise in data, we also average the flow rate calculated at different y positions. Formally, our channel flow rate is defined as

$$\phi = \langle Q_y \rangle = \frac{1}{L} \int_0^L Q_y dy, \quad (1)$$

where $Q_y = \int_{x_1}^{x_2} v_y(x, y) dx$ is the flow rate at y position, L is the length of the cropped image, and x_1 and x_2 are the left and right boundaries of the channel, respectively.

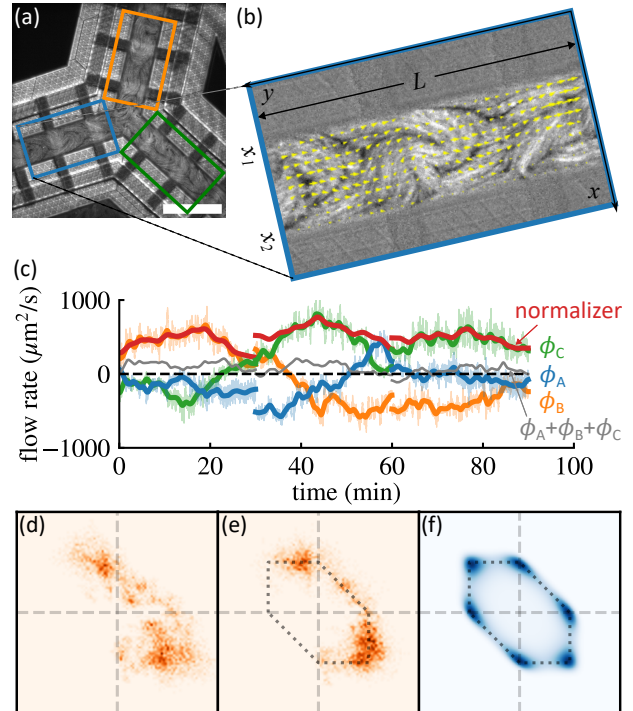


FIG. 2. Flow rate measurements and flow rate histogram. (a) A snapshot of microtubule-kinesin system confined in bifurcation channels. The scale bar is 200 μm. The rectangles indicate the regions where PIV analysis was performed. (b) Zoom-in view of channel A, yellow arrows indicates local velocity from PIV analysis. (c) Flow rate time series in the 3 channels A (blue), B (orange) and C (green). The light curves in the back are the real flow rates, while the bold curves in the front are Gaussian-smoothed flow rates with $\sigma = 50$ s. The “normalizer” and the sum of all flow rates are shown as red and gray, respectively. (d-f) Raw, normalized and theoretical flow rate histograms of channels B (vertical) and C (horizontal).

For consistency, we always define positive flow rate as the flow away from the connecting node. With this definition, the mass conservation at the connecting node can be expressed as $\phi_A + \phi_B + \phi_C = 0$.

The flow rates in channels A, B and C over time are plotted in Fig. 2(c) in blue, orange and green curves, respectively, corresponding to the colors of the rectangles in Fig. 2(a). The light curves in the back are the real flow rates, while the bold curves in the front are Gaussian-smoothed flow rates with $\sigma = 25$ s. The gray curve is the sum of the flow rates in the 3 channels, $\phi_A + \phi_B + \phi_C$, which serves as a check for mass conservation. The magnitude of the gray curve is much smaller than the flow rates in the 3 channels, indicating that mass conservation is indeed satisfied at the connecting node. Figures 2(d) show the histograms of raw flow rates in channels B and C. Darker colors indicate higher probability of flow rate configurations, and the crossing points of the dashed lines are the origin of the histogram ($\phi_B = \phi_C = 0$). We only show the histogram of the

flow rates in channels B and C, because the flow rates are constrained by $\phi_A + \phi_B + \phi_C = 0$, meaning that two flow rates are enough to specify the flow configuration. Since we were interested in the flow configurations, that is, how a flow in one channel was distributed in the other two channels, we focused on the normalized flow rates $\tilde{\phi}_A$, $\tilde{\phi}_B$ and $\tilde{\phi}_C$. This eliminated the effect of the fluctuating overall flow rates (for detailed normalization procedure, see Supplemental Information). The normalized flow rate histograms are shown in Fig. 2(e). Flow configurations that conserve mass is indicated by elliptic hexagons in dotted lines. The normalized flow rate histogram show good agreement with the mass conservation line, which is reassuring for our experimental and analytical techniques. It is possible to obtain the theoretical flow rate histogram by solving the Landau-type model proposed by Woodhouse and Dunkel [7]. In short, the model states that the flow in a channel network tends to minimize the total energy of the system, which comprises channel flow energy, diode energy and mass conservation energy. Formally, the Hamiltonian of the system to be minimized is

$$H = H_{\text{channel}} + H_{\text{diode}} + H_{\text{mass}}, \quad (2)$$

the detailed form of the Hamiltonian can be found in the original paper [7] and [Supplemental Information](#). By simulating the flow configurations in a Monte Carlo process, we obtained a theoretical flow rate histogram, as shown in Fig. 2(f). Compared to the theoretical flow rate histogram in Fig. 2(f), the experimental histogram shows a broader distribution, covering most of the possible configurations of flow rates in the 3 channels. Sharp peaks at polarized flow configurations, where one of the channels is a completely frustrated, however, were not observed in our experiment. It is worth noting that although the channels were designed to be fully symmetric, the grid requires a base structure to which the micromanipulator is attached (see Fig. 1(c)), which may result in asymmetry in the flow rates. This is probably the reason why we did not observe all the flow configurations that satisfy mass conservation, especially those where the flow in channel A goes outwards ($\phi_A > 0$).

B. Asymmetry in channel length

Channel length plays a crucial role in determining the flow behavior in channel networks, according to the theoretical model by Woodhouse and Dunkel [7]. Longer channels have a deeper energy well, which favors the flow to follow the longer path. To test this hypothesis, we designed a bifurcation channel system with two outlet channels of different lengths, as shown in Fig. 3(a) and sketched in Fig. 3(b). Channel A is modified with ratchets to ensure that channel A is always the inlet channel. Channel B is 1500 μm long, while channels A and C are both 500 μm long. All the channels have the same mean width of 150 μm . The flow rates in the 3 channels are

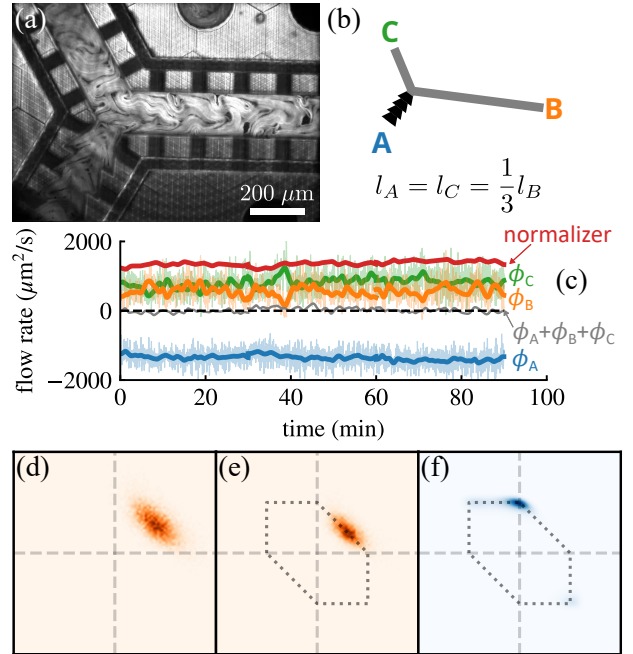


FIG. 3. Straight channel length effect. (a) A confocal fluorescence image of a bifurcation channel system with a 4-teeth ratchet inlet channel A and two straight outlet channels B and C with different lengths. The mean width of all channels is 150 μm . (b) A schematic diagram of the bifurcation channel system. The lengths of channel B is 1500 μm and the lengths of channels A and C are both 500 μm . (c) The time series of flow rates in all channels. The normalizer and the sum of all flow rates are shown as red and gray, respectively. (d) The flow rate histogram of channels B (vertical) and C (horizontal). The limits of the histogram are set to $[-2000, 2000]$ for both axes. (e) The normalized flow rate histogram. The limits of the histogram are set to $[-2, 2]$ for both axes. The hexagon in dotted lines indicates the configurations that conserve mass. (f) The theoretical flow rate histogram.

shown in Fig. 3(c). The ratchet structure is effective in polarizing the flow, as the flow rate in channel A is always negative, meaning that the flow is always directed towards the center node. At the bifurcation, neither of the outlet channels is apparently preferred. Instead, the flow splits almost equally between the two outlet channels. The shorter channel, C, has a slightly higher flow rate than the longer channel, B. This flow configuration is visualized in the raw and normalized flow rate histogram in Fig. 3(d) and (e), respectively. The prediction from the theoretical model is shown in Fig. 3(f), where a sharp peak is observed at the polarized flow configuration, showing a sharp contrast to the experimental result. This result shows that the longer path is not necessarily preferred.

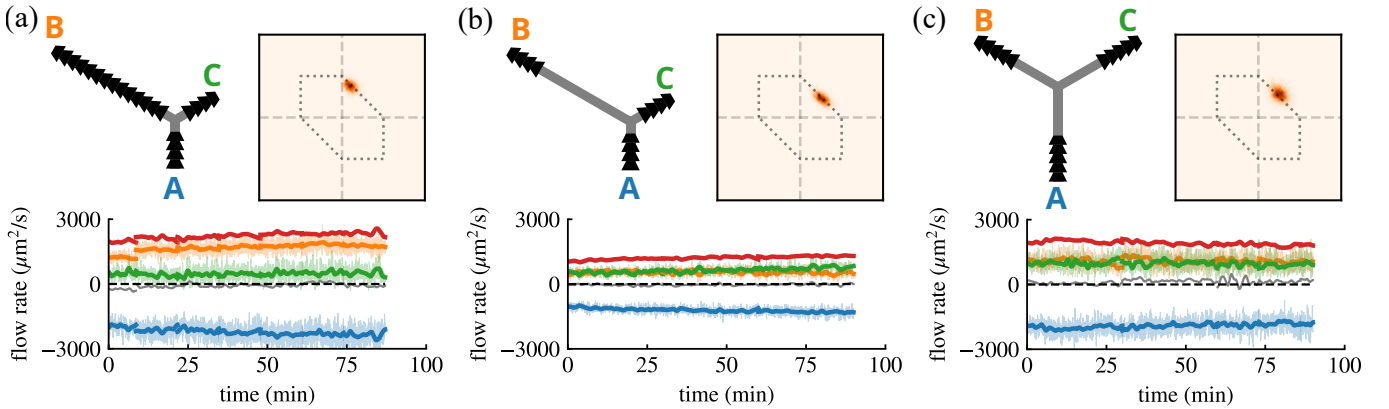


FIG. 4. Ratchet inlet and outlets: histogram and time series. (a) The numbers of ratchet teeth in channels A, B and C are 4, 14 and 4, respectively. The splitting ratio is around 3:1. (b) 4-4-4 bifurcation, where channel B has an extended straight portion. The flows again exhibit a sharp peak in the histogram at a splitting ratio around 1:1. (c) 5-5-5 bifurcation, where all the channels are of the same length. The flows again exhibit a sharp peak in the histogram at a splitting ratio around 1:1.

C. Ratchet inlet and outlets

The result from the asymmetric channel length experiment suggests that the ratchet structures play a more dominant role than channel length. We therefore use ratchet structures to modify both the inlet and outlet channels. The numbers of ratchet teeth and the length of non-ratchet parts are varied to study their effects on the flow behavior. All the experimental results, including flow rate time series and normalized histograms, are shown in Fig. 4. A general observation is that, in contrast to straight channel bifurcation systems, the flows exhibit a sharp peak in the histogram, indicating that the flow configurations are more deterministic and stable. When the outlet channels have different numbers of ratchet, as the channel system shown in Fig. 4(a), the flow robustly splits into different fractions in the two outlet channels. Interestingly, the flow rate ratio in the two outlet channels is almost equal to the ratio between the number of ratchet teeth.

Does this unequal splitting of flow arise from the difference in the length of the channels? To answer this question, we keep the channels lengths unchanged, but modify the number of ratchet teeth in channel B, so that channels B and C has the same number of ratchet teeth. In this case, the flow robustly split into the two outlet channels with a 1:1 ratio, as shown in Fig. 4(b). This result suggests that the ratchet teeth in the outlet channels play a dominant role in determining the splitting ratio at bifurcations.

Does the length of the straight part of the outlet channels matter? To answer this question, we further modify the channel system in Fig. 4(b) by make the length of the straight part of all the three channels identical, as shown in Fig. 4(c). The flow again splits with a 1:1 ratio, confirming the dominant role of ratchet teeth.

D. Defect dynamics: wall-slip and ratchet pinning

The dynamics of topological defects near the channel wall may provide insights into the steering mechanism of the ratchet structures, as well as the difference between the flow in straight and ratchet channels. In ratchet channels, $+1/2$ defects are observed to constantly form at the indentations on the channel walls, as shown in Fig. 5(a). All these $+1/2$ defects are pinned for around 10 seconds, before turning and merging with the main channel flow. These pinned defects are prohibited from moving further, and the extensile active stress generated by the kinesin motors drives the microtubules outside the indentations to flow in a consistent direction. [See supplemental video ratchet flow \(08_A\)](#). This wall pinning phenomenon is similar an earlier observation in a circular well [20]. The difference is that in the present work, the indentation is made asymmetric, thus setting a preferred flow direction. The kymograph in Fig. 5(a) also verifies the constant formation and pinning of the $+1/2$ defects. $+1/2$ defects also form in straight channels and move to the channel walls. However, they are not pinned on the walls, but can instead slip along the walls, as shown in the kymograph in Fig. 5(b), by the dark lines alternating between up and down motions. [See supplemental video straight flow \(09_A\)](#). This difference in wall defect dynamics may explain why ratchet channels play a more dominant role in determining the flow behavior at bifurcations.

E. Frustrated flow states

Flow frustrations are induced by coupling multiple channels with spontaneous flows, and are characteristic to active flow networks [15, 21]. In the fully ratchet asymmetric channel system, we clearly observed a frustrated flow state in the shorter channel. A close up view of the

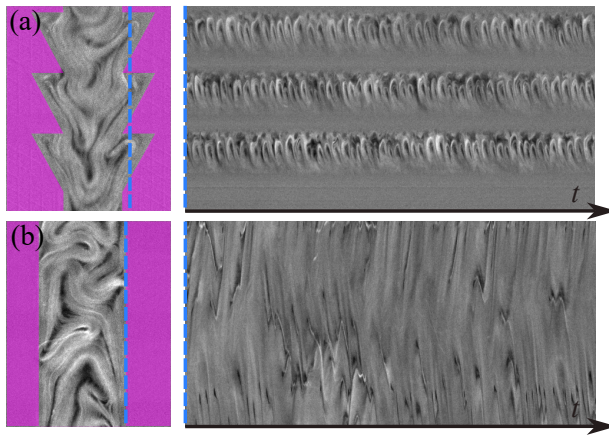


FIG. 5. Wall defect dynamics. (a) A snapshot of the active nematic flow in a ratchet channel and the kymograph at the blue dashed line. (b) A snapshot of the active nematic flow in a straight channel and the kymograph at the blue dashed line.

orientational ordering in the active nematics is shown in Fig. 6.

-
- [1] H Wioland, E Lushi, and R E Goldstein. Directed collective motion of bacteria under channel confinement. *New Journal of Physics*, 18(7):075002, July 2016. ISSN 1367-2630. doi:10.1088/1367-2630/18/7/075002.
- [2] Kun-Ta Wu, Jean Bernard Hishamunda, Daniel T. N. Chen, Stephen J. DeCamp, Ya-Wen Chang, Alberto Fernández-Nieves, Seth Fraden, and Zvonimir Dogic. Transition from turbulent to coherent flows in confined three-dimensional active fluids. *Science*, 355(6331):eaal1979, March 2017. ISSN 0036-8075, 1095-9203. doi:10.1126/science.aal1979.
- [3] Alexandre Morin and Denis Bartolo. Flowing Active Liquids in a Pipe: Hysteretic Response of Polar Flocks to External Fields. *Physical Review X*, 8(2):021037, May 2018. doi:10.1103/PhysRevX.8.021037.
- [4] Jérôme Hardouin, Rian Hughes, Amin Doostmohammadi, Justine Laurent, Teresa Lopez-Leon, Julia M. Yeomans, Jordi Ignés-Mullol, and Francesc Sagués. Reconfigurable flows and defect landscape of confined active nematics. *Communications Physics*, 2(1):121, December 2019. ISSN 2399-3650. doi:10.1038/s42005-019-0221-x.
- [5] Jérôme Hardouin, Justine Laurent, Teresa Lopez-Leon, Jordi Ignés-Mullol, and Francesc Sagués. Active microfluidic transport in two-dimensional handlebodies. *Soft Matter*, 16(40):9230–9241, 2020. ISSN 1744-683X, 1744-6848. doi:10.1039/D0SM00610F.
- [6] Sumesh P. Thampi. Channel confined active nematics. *Current Opinion in Colloid & Interface Science*, 61:101613, October 2022. ISSN 1359-0294. doi:10.1016/j.cocis.2022.101613. URL <https://www.sciencedirect.com/science/article/pii/S1359029422000528>.
- [7] Francis G. Woodhouse and Jörn Dunkel. Active matter logic for autonomous microfluidics. *Nature Communications*, 8(1):15169, April 2017. ISSN 2041-1723. doi:10.1038/ncomms15169.
- [8] Enkeleida Lushi, Hugo Wioland, and Raymond E. Goldstein. Fluid flows created by swimming bacteria drive self-organization in confined suspensions. *Proceedings of the National Academy of Sciences*, 111(27):9733–9738, July 2014. ISSN 0027-8424, 1091-6490. doi:10.1073/pnas.1405698111.
- [9] Zhengyang Liu, Kechun Zhang, and Xiang Cheng. Rheology of bacterial suspensions under confinement. *Rheologica Acta*, 58(8):439–451, August 2019. ISSN 0035-4511, 1435-1528. doi:10.1007/s00397-019-01155-x.
- [10] Tyler D. Ross, Heun Jin Lee, Zijie Qu, Rachel A. Banks, Rob Phillips, and Matt Thomson. Controlling organization and forces in active matter through optically defined boundaries. *Nature*, 572(7768):224–229, August 2019. ISSN 0028-0836, 1476-4687. doi:10.1038/s41586-019-1447-1.
- [11] R Voituriez, J. F Joanny, and J Prost. Spontaneous flow transition in active polar gels. *Europhysics Letters (EPL)*, 70(3):404–410, May 2005. ISSN 0295-5075, 1286-4854. doi:10.1209/epl/i2004-10501-2.
- [12] Davide Marenduzzo. Hydrodynamics and Rheology of Active Liquid Crystals: A Numerical Investigation. 98: 118102, 2007. doi:10.1103/PhysRevLett.98.118102.
- [13] Tyler N. Shendruk, Amin Doostmohammadi, Kristian Thijssen, and Julia M. Yeomans. Dancing disclinations in confined active nematics. *Soft Matter*, 13(21):3853–3862, May 2017. ISSN 1744-6848. doi:10.1039/C6SM02310J.
- [14] Jaideep P. Vaidya, Tyler N. Shendruk, and Sumesh P. Thampi. Active nematics in corrugated channels. *Soft Matter*, September 2024. ISSN 1744-6848. doi:10.1039/D4SM00760C. URL <https://pubs.rsc.org/en/content/articlelanding/2024/sm/d4sm00760c>. Publisher: The Royal Society of Chemistry.
- [15] Camille Jorge, Amélie Chardac, Alexis Poncet, and Denis Bartolo. Active hydraulics laws from frustration principles. *Nature Physics*, 20(2):303–309, February 2024. ISSN 1745-2481. doi:10.1038/s41567-023-02301-2. URL <https://www.nature.com/articles/s41567-023-02301-2>. Publisher: Nature Publishing Group.

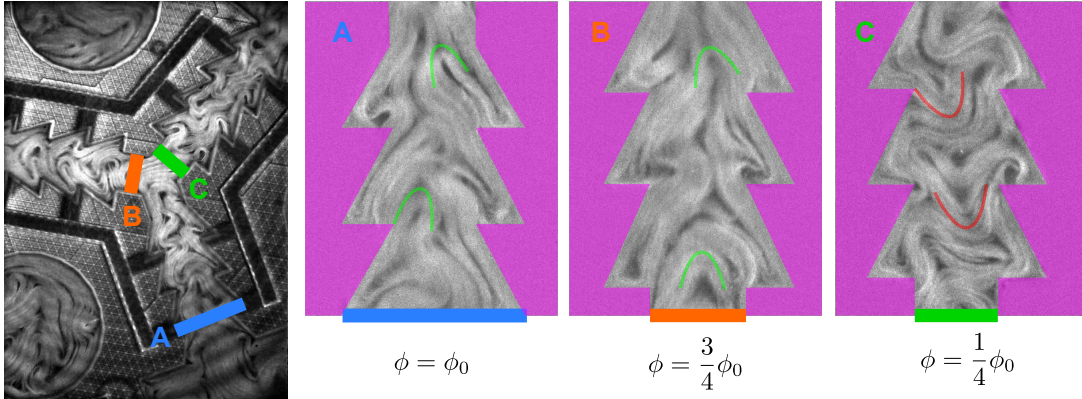


FIG. 6. Frustrated flow state. Active nematic orientational ordering at the bifurcation. The channel system is the same as in Fig. 3(a), where the flow comes in from channel A at $\phi = \phi_0$ and splits into channels B and C with splitting ratio around 3:1. On the right, we show the close up views of the active nematics to highlight the difference in the orientational ordering in normal normal flow state (channels A and B) and frustrated flow state (channel C).

- [16] S. Elizabeth Hulme, Willow R. DiLuzio, Sergey S. Shevkoplyas, Linda Turner, Michael Mayer, Howard C. Berg, and George M. Whitesides. Using ratchets and sorters to fractionate motile cells of *Escherichia coli* by length. *Lab on a Chip*, 8(11):1888, 2008. ISSN 1473-0197, 1473-0189. doi:10.1039/b809892a. URL <https://xlink.rsc.org/?DOI=b809892a>.
- [17] R. Di Leonardo, L. Angelani, D. Dell'Arciprete, G. Ruocco, V. Iebba, S. Schippa, M. P. Conte, F. Mecarini, F. De Angelis, and E. Di Fabrizio. Bacterial ratchet motors. *Proceedings of the National Academy of Sciences*, 107(21):9541–9545, May 2010. ISSN 0027-8424, 1091-6490. doi:10.1073/pnas.0910426107.
- [18] Sattvic Ray, Jie Zhang, and Zvonimir Dogic. Rectified Rotational Dynamics of Mobile Inclusions in Two-Dimensional Active Nematics. *Physical Review Letters*, 130(23):238301, June 2023. ISSN 0031-9007, 1079-7114. doi:10.1103/PhysRevLett.130.238301. URL <https://link.aps.org/doi/10.1103/PhysRevLett.130.238301>.
- [19] Tim Sanchez, Daniel T. N. Chen, Stephen J. DeCamp, Michael Heymann, and Zvonimir Dogic. Spontaneous motion in hierarchically assembled active matter. *Nature*, 491(7424):431–434, November 2012. ISSN 0028-0836, 1476-4687. doi:10.1038/nature11591.
- [20] Jérôme Hardouin, Claire Doré, Justine Laurent, Teresa Lopez-Leon, Jordi Ignés-Mullol, and Francesc Sagués. Active boundary layers in confined active nematics. *Nature Communications*, 13(1):6675, November 2022. ISSN 2041-1723. doi:10.1038/s41467-022-34336-z. URL <https://www.nature.com/articles/s41467-022-34336-z>. Publisher: Nature Publishing Group.
- [21] Kazusa Beppu, Kaito Matsuura, and Yusuke T. Maeda. Geometric frustration and pairing-order transition in confined bacterial vortices. *Physical Review Research*, 6(3):033166, August 2024. doi:10.1103/PhysRevResearch.6.033166. URL <https://link.aps.org/doi/10.1103/PhysRevResearch.6.033166>. Publisher: American Physical Society.